Wideband and Tunable Reflective Cross-Polarization Conversion Metasurface for TeraHertz Applications

K. B. S. Sri Nagini, *Graduate Student Member, IEEE*, and Chandu DS 🆔, *Member, IEEE*

Abstract—An ultrathin and wideband reflective cross-polarization converter is presented in this paper. The design consists of a pair of modified dumbbell shaped resonators which are connected together with a conductive strip. The proposed single-layer THz metasurface achieved a high polarization conversion ratio (PCR) of $\geq 95\%$ in the operating frequency ranging from 1.76–4.26 THz. This wide-bandwidth cross-polarization conversion is obtained by exciting multiple closely spaced resonant frequencies at 1.98 THz, 2.61 THz, 2.95 THz, and 3.93 THz. The working mechanism of the proposed structure is analyzed and the polarizer exhibits an excellent angular stability upto 40^0 of incidence. Further, the proposed cross-polarizer exhibits continuous tunability of PCR over the operating frequencies when photoconductive silicon (Si) is filled in the gap between pair of dumbbell-resonators. The wideband characteristics and the switchable property show that the proposed reflective cross polarizer is an excellent candidate for manipulation and control of polarization in THz communication systems.

Index Terms—Cross-polarization, metasurface, polarization conversion ratio (PCR), switchable, wideband.

I. INTRODUCTION

WITH the advancement of communication systems and the growing demand for ultra high speed communications, the electronics and photonics communities are witnessing the emergence of waveguides, filters, sensors, amplifiers, polarization converters, etc in the THz regime (around 0.1 - 10 THz) for a variety of applications including imaging [1], [2], [3], sensing [4], [5], [6], and communications [7], [8], [9]. However, there is a limited research in the development of wideband polarization converters together with dynamically controlling the polarization state of THz waves.

Metasurfaces employing sub-wavelength resonant structures are widely being used for polarization control purposes. In the literature, metasurface polarization converters have been designed based on transmissive mode [10], [11], [12], [13], [14], transmissive and reflective mode [15] and reflective modes [16], [17], [18], [19], [20], [21], [22], [23], [24], [25], [26], [27], [28]. The transmissive type polarization converters suffer due to narrow bandwidth [13], [14] or require multilayer topologies to provide wideband operation [11]. On the other hand, the

reflective type polarizers have significant anisotropic properties compared to transmissive polarizers [29], [30] and the resonator approach is the most sought method to realize wideband frequency response. There are several techniques to excite multiple modes of the resonator to achieve wideband response. In [16], a reflective cross-polarizer is designed based on conventional split ring resonator with the combination of metallic disks and achieved 0.8 THz bandwidth due to the superposition of three resonance modes at 0.71 THz, 0.99 THz, and 1.37 THz. The same idea was extended in [17] to realize four resonant modes and achieved greater bandwidth ranging from 0.65-1.58 THz. However, because of the highly resonant characteristics of the split-ring, the polarization conversion ratio (PCR) is limited to only 80% in these works. In [19], [20], an array of H-shaped unit cell structures are introduced for reflecting phases, resulting in cross- polarization conversion bandwidth of 0.2 THz and 0.3 THz, respectively. The PCR of these reported works are $\geq 85\%$. But, owing to the dielectric losses, it is observed that there is a trade-off between wide angle of incidence and broad bandwidth, and it is difficult to sustain the PCR for larger incidence angles. To overcome this issue, a broadband THz cross-polarization converter is designed based on low loss dielectric layers and T-shaped resonators which achieved a stable bandwidth of 0.72 THz (0.36-1.08 THz) up to 45° angle of incidence [18]. To achieve tunability of PCR, a center-cut cross shaped resonator has been designed in which the gap is filled with photoconductive silicon (Si) [21]. This reflective cross-polarizer achieved high polarization efficiency of $> 95\%$ over a significant bandwidth of 1.08 THz. On the other hand, without center-cut for the cross shaped resoantor and using graphene for tunability [22], the bandwidth was enhanced up to 1.85 THz in the operating band of 2.15-4 THz. However, the minimum PCR reduced to 80%, thereby justifying that there is a trade-off between the wide polarization bandwidth and PCR. In order to achieve simultaneous enhancement in bandwidth and PCR, a reflective cross-polarizer has been designed using anchor-shaped resonator [23]. This structure realizes a bandwidth of 1.62 THz by the combination of two resonant frequencies at 1.34 THz and 2.06 THz with a conversion efficiency greater than 93%. Gradient structures and multi-layered polarizers have also resulted in wide cross-polarization bandwidth [24], [25], [26]. For example, the combination of a rectangular-shaped resonator and a circular-shaped resonator employing graphene for tunability [26] resulted in a record bandwidth enhancement up to 2.51 THz, but at a minimum PCR of only 80%. All of the reported works either have a narrow bandwidth with a high PCR ($\geq 90\%$), or designed

The authors are with the School of Electronics Engineering, VIT-AP University, Amaravati 522 237, India (e-mail: srinagini.21phd7012@vitap.ac; cds.iiitdm@gmail.com).
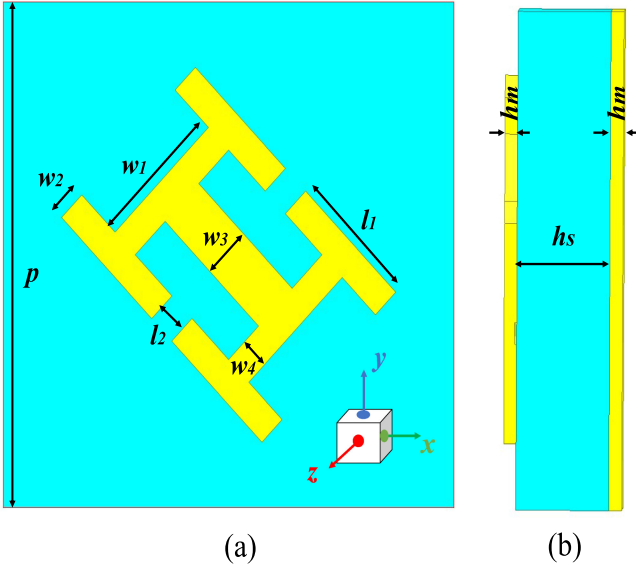
Fig. 1. Geometry of the unit cell. (a) top-view and (b) side-view.

Fig. 2. Fabrication process of the polarization converter.

on a thicker substrate or do not support tunability. Therefore, designing a low profile wideband THz reflective cross-polarizer with a high PCR and switchable characteristics is still an open challenge for research.

In this paper, a switchable wideband reflective cross-polarization converter operating in the THz region is proposed. The cross-polarizer in this work consists of a periodic array of modified dumbbell-shaped resonators connected with conductive strip. Photoconductive silicon is filled in the gap between dumbbell resonators. The designed structure achieves wideband cross-polarization conversion from 1.76–4.26 THz and a high polarization conversion efficiency of 95% with ON and OFF states. In the following sections, the proposed structure and its working principle are described in detail.

II. POLARIZATION CONVERTER DESIGN

A. Unit Cell Geometry and Fabrication

The geometry of the unit cell of the proposed reflective cross-polarization converter is shown in Fig. 1(a) and it's side-view is shown in Fig. 1(b). The top layer of the unit cell consists of modified dumbbell-shaped resonators connected together by a metallic strip. These metallic structures along with the ground plane at the bottom layer are made up of gold with a conductivity (σ) of 4.56×10^7 S/m and a thickness (h_m) of 0.2 μm. The middle layer is a 15 μm thick (h_s) polydimethylsiloxane (PDMS) substrate with a relative permittivity (ϵ_r) of 2.7 and a dielectric loss tangent of 0.02. The optimized parameters of the unit cell are as follows: periodicity (p) =48, $l_1 = 13.5$, $l_2 = 3$, $w_1 = 14$, $w_2 = 3$, $w_3 = 5$ and $w_4 = 3$ (all the dimensions are in μm).

The dimensions of the polarization converter make the structure suitable for fabrication using the well-known micro-fabrication process. The steps in the fabrication of the polarization converter are illustrated in Fig. 2 and can be described as
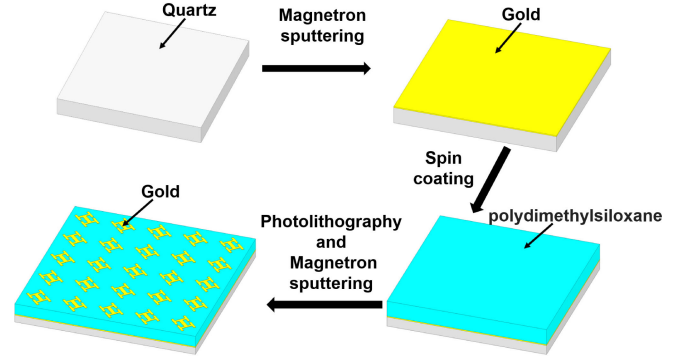
follows: Initially, quartz is taken as a carrier substrate and 0.2 μm (h_m) thick layer of gold is magnetron-sputtered on the quartz wafer. Later, a 15 μm (h_s) thick layer of PDMS is spin-coated onto the reflecting gold layer. The metallic patterns on top of PDMS are deposited using photolithography followed by magnetron sputtering. Firstly, two layers of photoresist (AZ1500 series on top of LOR) are spin-coated onto the PDMS surface. The photoresist is then exposed to UV light passing through the mask while the non-masked part was washed away with the developing solution to obtain the pattern. Subsequently, a 0.2 μm (h_s) thick layer of gold is deposited on the exposed photoresist using magnetron sputtering. Finally, the reflecting layer, substrate and the metallic pattern in the top-plane are peeled off from the carrier substrate to realize the proposed structure.

B. Working Principle

Simulations are carried out in order to understand the working principle of the metasurface. For the proposed unit cell, periodic boundary conditions are applied along the x and y directions, while the open space boundary condition is applied along the $+z$ direction. A linearly polarized plane wave is incident along the $+z$ direction and the simulation was performed using commercial full-wave simulator to obtain the magnitude and phase of the reflection coefficients. Consider a y-polarized EM wave incident on the unit cell as shown in Fig. 3. It is decomposed into two orthogonal components: u-component along the u-axis and v-component along the v-axis. The u-and v-axes are oriented at 45° anti-clockwise with respect to x-and y-axis, respectively.

From Fig. 3, E_{iu} and E_{iv} are the incident electric field components along u- and v-axis, respectively. The incident y-polarized wave can now be represented as

$$E_i = \hat{y}E_i e^{-jkz} = (\hat{u}E_{iu} + \hat{v}E_{iv})e^{-jkz} \qquad (1)$$

At $z = 0$,

$$E_i = \hat{y}E_i = (\hat{u}E_{iu} + \hat{v}E_{iv}) \qquad (2)$$

Similarly, the reflected wave E_r from the polarizer at $z = 0$ in terms of reflected electric field components E_{ru} along u-axis and E_{rv} along v-axis, can be represented as
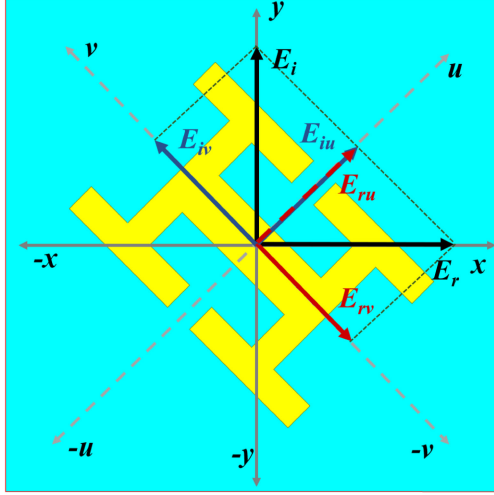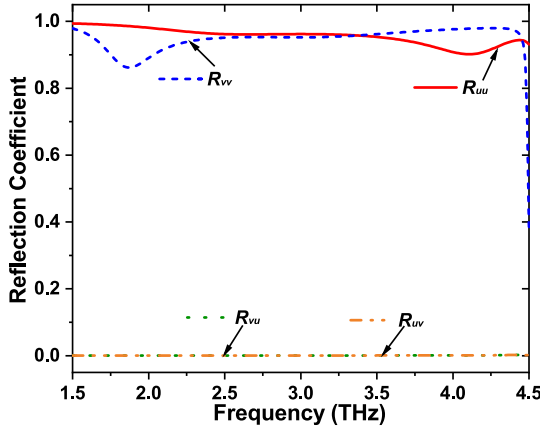
$$E_r = (\hat{u}E_{ru} + \hat{v}E_{rv}) \qquad (3)$$

Fig. 3. Decomposition of electric field components.

Fig. 5. Phase difference between *u* and *v*-polarized waves.

Fig. 4. Magnitude of reflection coefficients for *u* and *v*-polarization.
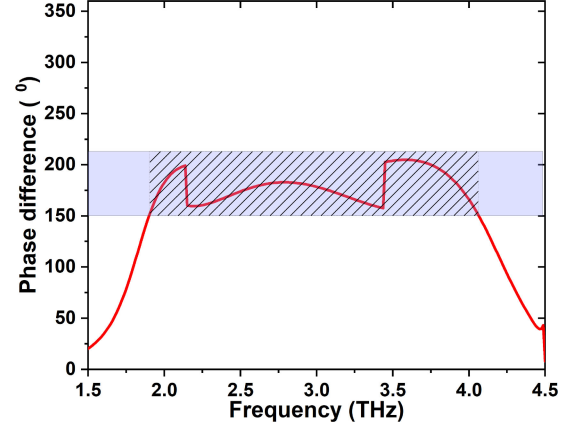
In terms of the reflection of decomposed co-polarization components (R_{uu}, R_{vv}) and cross-polarization components (R_{uv}, R_{vu}) along *u* and *v*-axes and the phase differences between the corresponding components (ϕ_{uu}, ϕ_{vv}, ϕ_{uv} and ϕ_{vu}), the reflected wave E_r from the polarizer is

$$E_r = \hat{u}(R_{uu}E_{iu}e^{j\phi_{uu}} + R_{uv}E_{iv}e^{j\phi_{uv}})$$
$$+ \hat{v}(R_{vu}E_{iu}e^{j\phi_{vu}} + R_{vv}E_{iv}e^{j\phi_{vv}}) \quad (4)$$

For cross-polarization conversion, the reflected wave has to be *x*-polarized. This can be achieved under two conditions:

Condition 1: The co-polarization and cross-polarization reflection components along the *u*- and *v*-axes should have magnitudes $|R_{uu}| = |R_{vv}| \approx 1$ and $|R_{uv}| = |R_{vu}| \approx 0$, respectively. This can be verified from Fig. 4 where the magnitudes of R_{uu} and R_{vv} are close to unity and the magnitudes of R_{uv} and R_{vu} are almost zero, satisfying this theoretical condition. So, from (4), the reflected wave now becomes,

$$E_r = \hat{u}E_{iu}e^{j\phi_{uu}} + \hat{v}E_{iv}e^{j\phi_{vv}} \quad (5)$$

Condition 2 : The proposed polarizer should satisfy the orthogonality condition ($E_i.E_r = 0$) between the incident and reflected waves for cross polarization conversion. From (2) and (5), this orthogonality condition leads to a relation $|(\phi_{vv} - \phi_{uu})| = 180°$. To verify this, the phase difference between the co-polarized reflected waves in the *u*- and *v*- axes of the polarizer is plotted as shown in Fig. 5. In general, a phase difference of 180° $\pm 30^0$ between the *u* and *v*- reflection components is considered acceptable for cross-polarization conversion [31]. It can be observed (from the hatched area) that the phase difference of $180° \pm 30^0$ is maintained over a wide range of frequencies from 1.76-4.26 THz. Structurally, the proposed polarizer is asymmetric and obeys anisotropic properties. Due to this, the electric field components E_{ru} and E_{iu} are in the same direction, whereas the electric field components E_{rv} and E_{iv} are in opposite direction leading to a phase difference of 180° between R_{uu} and R_{vv}. Therefore, according to the orthogonality condition and from Fig. 4, it can be observed that for a *y*-polarized incident wave, the direction of the reflected wave is along the *x*-axis and hence the proposed metasurface converter exhibits the cross-polarization conversion.

In order to study the polarization purity and the efficiency of the proposed polarizer, the co-polarized (R_{yy}) and cross-polarized (R_{xy}) reflection coefficients are plotted in Fig. 6. The polarization converter exhibits four resonant frequencies at 1.98 THz, 2.61 THz. 2.95 THz and 3.93 THz. It can be observed that the co-polarization (cross-polarization) reflected component has the magnitudes of 0.94 (0.05), 0.94 (0.16), 0.96 (0.001), and 0.95 (0.04) at the corresponding resonant frequencies. The magnitude of cross-polarization reflection coefficient ($|Rxy|$) is higher than 0.94 and the co-polarization reflection coefficient ($|Ryy|$) is equal to near zero in the wideband frequency range of 1.76–4.26 THz.

Using these results in eq. (6), the polarization conversion ratio is plotted in Fig. 7 to evaluate the efficiency of the proposed cross-polarization converter.

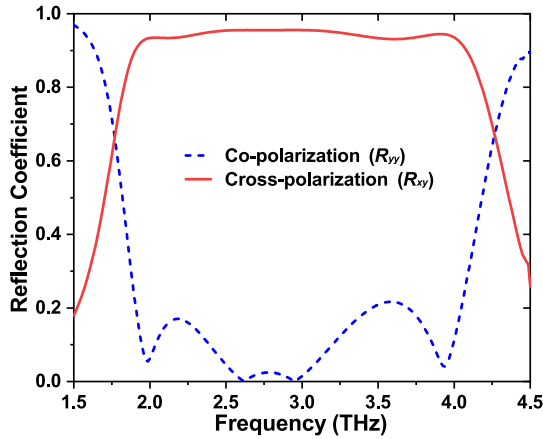$$PCR = \frac{|R_{xy}|^2}{|R_{xy}|^2 + |R_{yy}|^2} \quad (6)$$

Fig. 6. Magnitude of co and cross-polarized reflection coefficients for *x* and *y*-polarization.
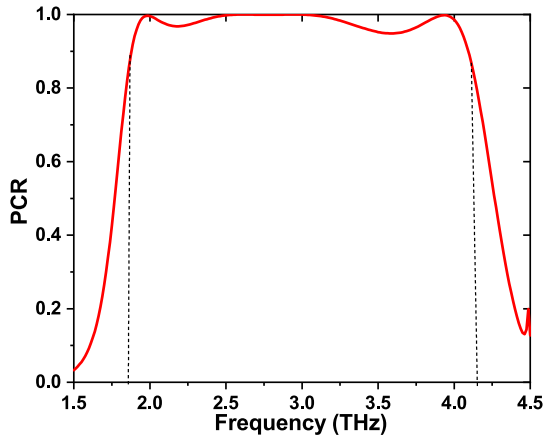

Fig. 7. PCR of proposed polarization converter.

At the resonant frequencies of 1.98 THz, 2.61 THz, 2.95 THz and 3.93 THz, the achieved PCR is 99.65%, 99.88%, 99.74% and 99.81% which signifies that the *y*-polarized incident wave is converted to an *x*-polarized reflected wave with an extremely good efficiency. Also, the PCR is greater than 95% over the frequency range from 1.76–4.26 THz.

C. Design Procedure

The design steps of proposed polarization converter are as follows. Firstly, as step 1 a pair of dumbbell-shaped resonators (Arm 1 and Arm 2) with single-sided bars offset from the center by $a = 10$ μm are designed as shown in Fig. 8. It can be observed from Fig. 9(a), that this structure resonates at 4.07 THz. The two dumbbell-shaped resonators are connected using a conductive strip of length $2a$ and width w_3 as shown in step 2. This connection puts together Arm 1 and Arm 2 as a single resonator resulting in a lower order resonant mode at 2.26 THz as shown in Fig. 9(b). It is worth mentioning that the frequency band due to Arm 1 and Arm 2 at 4.07 THz is preserved. This structure provides a dual-band response and it is evident that the magnitude of reflection coefficient in between 2.26-4.07 THz

is very poor. To futher better the reflection coefficient between the two existing resonant frequencies, a pair of dumbbell bars are added on top of Arm 1 and bottom of Arm 2. It can be observed that, when the gap between the bars of the dumbbell is optimized to l_2, better impedance matching is achieved and a pair of resonant modes occurs at 2.61 and 2.95 THz as shown in Fig. 9(c).

Thus, this structure provides four closely spaced resonant frquencies at 1.98 THz, 2.61 THz, 2.95 THz and 3.93 THz. The combination of these closely spaced modes results in wide-bandwidth for polarization conversion.

III. RESULTS AND DISCUSSION

To understand the physical mechanism of the proposed reflective cross-polarization converter, the surface current distributions at top and bottom planes of the THz metasurface are presented as shown in Fig. 10. At resonant frequencies $f_1 = 1.98$ THz and at $f_2 = 2.61$ THz, the surface currents on the top of the metallic conductor and bottom ground plane flow in opposite direction. As the directions of current are anti-parallel, it can be inferred that the cross-polarizer exhibits magnetic resonance at 1.98 and 2.61 THz. Also, most of the current is concentrated along the metallic strip which is responsible for the resonant frequency f_1 that can be observed from Fig. 10. At third and fourth resonant frequencies $f_3 = 2.95$ THz and $f_4 = 3.93$ THz, the flow of currents on the top and bottom plane are parallel, leading to electric resonance. It is also proved that the resonant frequency f_4 is because of the dumbbell strips of the resonator as high intensity current is concentrated at that region as seen in Fig. 10.

A. PCR Analysis

Metasurfaces are structure dependent and the PCR depends on the dimensions of the metasurface. Therefore, the effect of geometrical parameters on the PCR is analyzed by varying the width of the rectangular strip (w_3), the gap between the pair of dumbbells (l_2) and the width of the resonator arms. When the width of the rectangular strip (w_3) is increased from 3 to 7 μm, it is observed that the highest resonant frequency remains intact at 3.93 THz as shown in Fig. 11(a). Although the PCR is above 90% for $w_3 > 5$ μm, there is a significant red shift in the first resonant frequency from 1.76 to 1.84 THz, thereby reducing the effective cross-polarization bandwidth. On the other hand, when $w_3 < 5$ μm, the efficiency of polarization conversion is significantly effected falling down to $< 80\%$ when $w_3 = 3$ μm. Thus, for $w_3 = 5$ μm, the metasurface provides wide-bandwidth with highest PCR. On the other hand, when the gap between the dumbbells (l_2) is increased from 2 to 5 μm, the PCR is observed to be within the permissible limits ($> 90\%$). However, the PCR deteriorates rapidly when l_2 is reduced below 2 μm as shown in Fig. 11(b). The width of the dumbbell arm (w_4) has a severe effect on the highest operating frequencies. As shown in Fig. 11(c), when w_4 is increased, there is no change in the lowest resonant frequency, but, the PCR drops to 69% when the width of the arm is 5 μm. This is due to the blue shift in the upper resonant frequencies. Therefore, the optimized
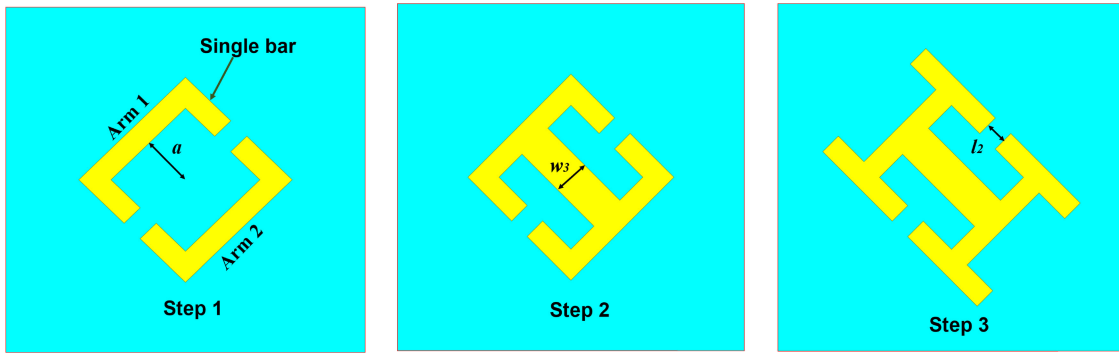
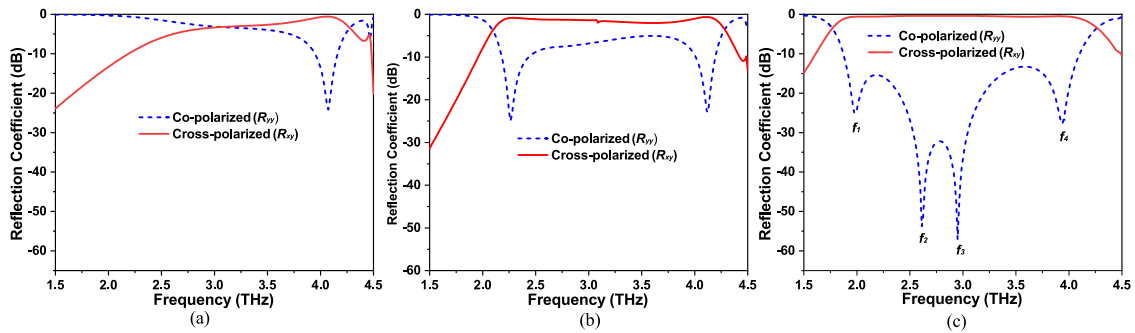Fig. 8. Design evolution of the proposed polarizer.
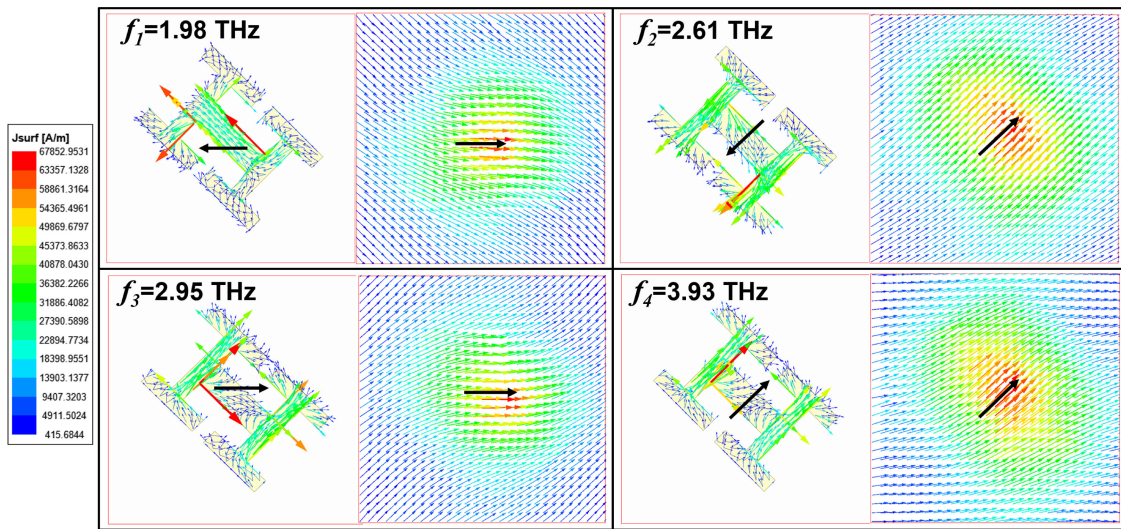

Fig. 9. Reflection coefficients based on design steps.

Fig. 10. Current distributions of the proposed structure at 1.98 THz, 2.61 THz, 2.95 THz and 3.93 THz.

value of w_4 is chosen as 3 μm to achieve maximum polarization conversion efficiency. Thus, the proposed polarization converter provides the optimization of the individual resonant frequencies by the proper choice of parameters of the metasurface structure.

The response of the polarizer is also analyzed for different angles of incidence as shown in Fig. 11(d). At low frequencies, below 3 THz, there is insignificant change in the polarization

efficiency up to $40°$ of incidence. However, at higher resonating modes above 3 THz, the polarizer is sensitive to the incidence angle and PCR of $>90\%$ is maintained up to $40°$ of oblique incidence. It is observed that the PCR bandwidth reduces beyond this incidence angle and the higher frequency is red shifted from 3.93 to 3.98 THz. Therefore, the proposed metasurface provides stable response up to an angle of $40°$ which makes it suitable for THz polarization-control applications.
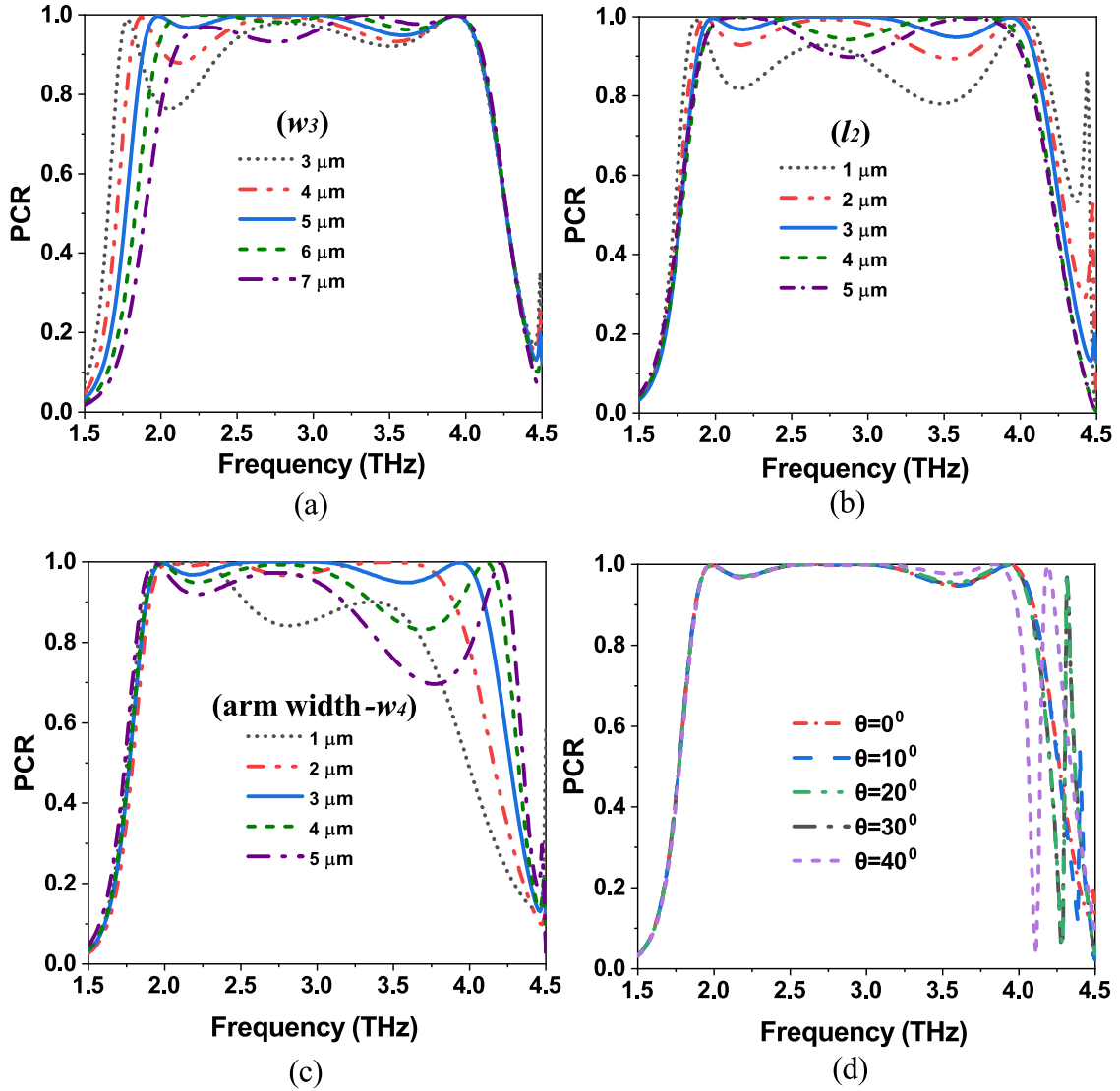
Fig. 11. PCR analysis with variation in (a) Width of the rectangular conductive strip, (b) gap between the dumbbells, (c) arm width of proposed polarization converter and (d) Stability analysis of PCR.

TABLE I
PERFORMANCE COMPARISON WITH EXISTING CROSS-POLARIZATION CONVERTERS

Ref	Design technique (Resonators)	Frequency range (THz)	Bandwidth (THz)	Thickness (μm)	PCR (%)	Stability (degrees)	Switchable (Yes / No)	Material $
[19]	H-shaped	0.4-0.6	0.2	75	95	NG	No	NA
[20]	H-shaped	0.35-0.65	0.3	75	85	NG	No	NA
[18]	T-shaped	0.36-1.08	0.72	79	80	45	No	NA
[16]	Split-ring	0.65–1.45	0.8	30	80	NG	No	NA
[17]	Split-ring	0.65-1.58	0.93	29	80	NG	Yes	Silicon
[32]	Crescent-shaped	0.64–1.47	0.83	37.5	90	30	Yes	Silicon
[33]	L-shaped	4.2-5.2	1	7	98	30	No	NA
[21]	Cross-shaped	1.86–2.94	1.08	16	95	NG	Yes	Silicon
[23]	Anchor-shaped	1.21-2.83	1.62	21	93	45	No	NA
[22]	Complementary cross-shaped	2.15-4	1.85	20	80	NG	Yes	Graphene
[24]	Butterfly-shaped	2.5-4.7	2.2	16	NG	NG	Yes	Graphene
[25]	Two disks and double-headed axe	1.35-3.55	2.2	17	90	NG	Yes	Graphene
[26]	phi-shaped	4.83–7.34	2.51	8.5	80	40	No	NA
TW*	**Modified dumbbell pair**	**1.76-4.26**	**2.5**	**15**	**95**	**40**	**Yes**	**Silicon**

*TW indicates this work, $ material used for tunability.
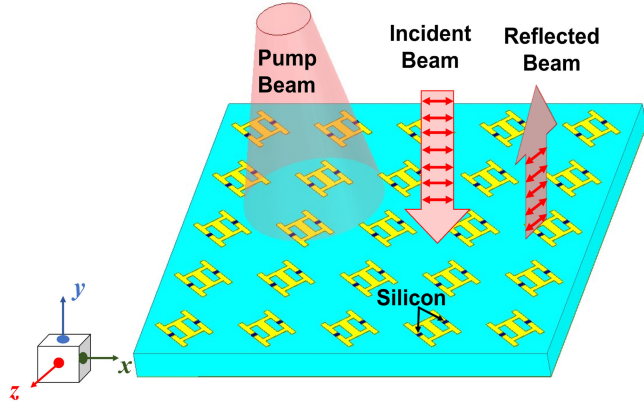
Fig. 12. Excitation using external optical pump on the array of the polarization converter.
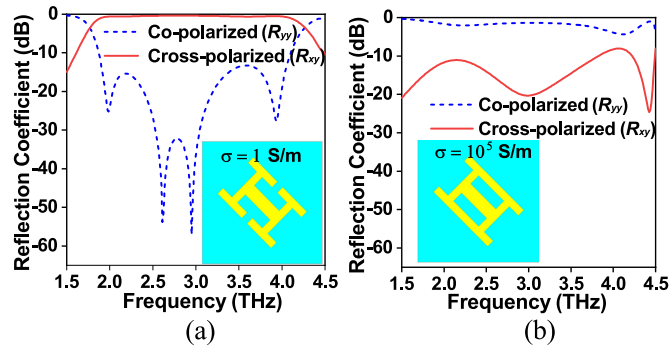

Fig. 14. Illustrtaion of tunability.

Fig. 13. Co-polarized and cross-polarized reflection coefficients for (a) $\sigma = 1$ S/m and, (b) $\sigma = 10^5$ S/m.

B. Tunability Analysis

Photoconductive silicon material of 3 μm $\times$ 3 μm is integrated in the gap (l_2) between the dumbbell resonators to obtain the switchable polarization conversion. Silicon is chosen over graphene for tunability because of it's high relative permittivity (ϵ_r) of 11.7 and low absorption loss at THz frequencies. To achieve tunability, the sample metasurface consisting of an array of periodic unit cells is initially subjected to external optical excitation as shown in Fig. 12. A continuous wave laser can be used to obliquely irradiate the entire area of the metasurface [34]. The dynamic changes in the conductivity of silicon is then observed by varying the optical pump beam power. When there is no optical illumination, silicon has minimum conductivity $\sigma = 1$ S/m and behaves as an insulator [35]. In this case, the photoconductive silicon essentially disconnects the dumbbell resonators, leaving a gap of l_2 between them. The unit cell in Fig. 12 is now equivalent to the proposed unit cell shown in the inset of Fig. 13(a). Therefore, the integrated metasurface provides the polarization conversion as per the discussion in Section-II and the polarizer is said to be in it's ON state and provides wideband cross-polarization conversion as shown in Fig. 13(a). When the pump beam energy is greater than the energy band gap of silicon, the carrier density in silicon increases and thereby it's conductivity increases. The maximum conductivity of the silicon
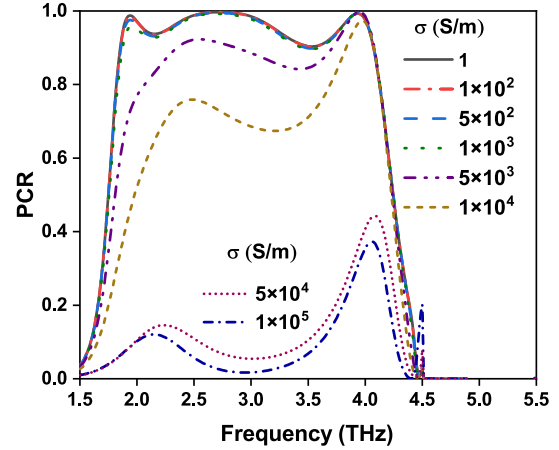
is 10^5 S/m due to the maximum limiting value of the energy flux of the pump [35]. At this maximum conductivity, silicon bridges the gap between the dumbbell resonators ($l_2 = 0$) as shown in the inset of Fig. 13(b). In this case, the magnitude of reflected co-polarized component (R_{yy}) is dominant than the reflected cross-polar component (R_{xy}) as shown in Fig. 13(b). Therefore, the integrated metasurface is said to be in OFF state and does not provide cross-polarization conversion. To further verify the same, as shown in Fig. 14, it is clear that the PCR is $\geq 80\%$ for the ON-state and $\leq 80\%$ for the OFF-state. Thus, integrating the structure with Si material provides the switching characteristics for the reflective polarization converter.

The performance comparison of the proposed reflective cross polarizer with the existing polarizers is listed in Table. I. The proposed structure exhibits superior performance compared with other existing reflective cross polarizers. Although the bandwidth of the structure in [26] is the highest, it was reported for a PCR of 80%. In this work, similar range of bandwidth is reported for PCR 95% The polarizer in [33] has the highest PCR of 98%, but the structure suffers from low bandwidth and limited angular stability. In summary, it can be observed that the proposed cross polarizer has wide bandwidth, high PCR, low profile and decent angular stability with switchable characteristics.

IV. CONCLUSION

A switchable reflective cross-polarization converter based on modified dumbbell-shaped resonators is proposed for THz applications. Wideband cross-polarization is achieved from 1.76-4.26 THz with PCR of $\geq 95\%$ and the proposed polarizer exhibits up to 40° of angular stability. Tunability of PCR is achieved by integrating photoconductive silicon in the polarization converter and varying the optical pump power. The polarization conversion mechanism is explained by using decomposition of electric field components. The design steps are discussed to elucidate the origin of closely spaced four resonant frequencies (1.98 THz, 2.61 THz, 2.95 THz, and 3.93 THz) for wideband response. The current distributions are illustrated for a better understanding of the principle of operation of cross polarization converter. The

proposed wideband cross poalrizer has potential applications in polarization control of THz waves in active switches, sensing and imaging.

REFERENCES

[1] R.-D. Li, B.-C. Yin, and B.-C. Ye, "Ultrasensitive, colorimetric detection of microRNAs based on isothermal exponential amplification reaction-assisted gold nanoparticle amplification," *Biosensors Bioelectron.*, vol. 86, pp. 1011–1016, 2016.

[2] R. M. H. Bilal, M. A. Baqir, P. K. Choudhury, M. M. Ali, and A. A. Rahim, "On the specially designed fractal metasurface-based dual-polarization converter in the THz regime," *Results Phys.*, vol. 19, 2020, Art. no. 103358.

[3] S. Watanabe, "Terahertz polarization imaging and its applications," *Photonics*, vol. 5, no. 4, 2018, Art. no. 58.

[4] Z. Zhang, T. Zhang, F. Fan, Y. Ji, and S. Chang, "Terahertz polarization sensing of bovine serum albumin proteolysis on curved flexible metasurface," *Sens. Actuator A: Phys.*, vol. 338, 2022, Art. no. 113499.

[5] C. Zhong, F. Fan, Z. Zhang, H. Liu, and S. Chang, "Terahertz polarization sensing based on the saccharide-PVA mixture film coated on the flexible metasurface sensor," *Opt. Lasers Eng.*, vol. 149, 2022, Art. no. 106798.

[6] D. Saeedkia, *Handbook of Terahertz Technology for Imaging, Sensing and Communications*. Amsterdam, The Netherlands: Elsevier, 2013.

[7] S.-Y. Zhu, G.-B. Wu, S. W. Pang, and C. H. Chan, "Compact terahertz dielectric folded metasurface," *Adv. Opt. Mater.*, vol. 10, no. 3, 2022, Art. no. 2101663.

[8] Y. Yang et al., "Terahertz topological photonics for on-chip communication," *Nat. Photon.*, vol. 14, no. 7, pp. 446–451, 2020.

[9] H. Zhao, X. Wang, B. Quan, S. Liu, and Y. Zhang, "High-efficiency phase and polarization modulation metasurfaces," *Adv. Photon. Res.*, vol. 3, no. 2, 2022, Art. no. 2100199.

[10] P. Das and K. Mandal, "Transmissive type dual band polarization converter integrated microstrip patch antenna in THz regime," *Optik*, vol. 261, 2022, Art. no. 169157.

[11] R. T. Ako, W. S. Lee, S. Atakaramians, M. Bhaskaran, S. Sriram, and W. Withayachumnankul, "Ultra-wideband tri-layer transmissive linear polarization converter for terahertz waves," *APL Photon.*, vol. 5, no. 4, 2020, Art. no. 046101.

[12] F. Lv, L. Wang, Z. Xiao, M. Chen, Z. Cui, and Q. Xu, "Asymmetric transmission polarization conversion of chiral metamaterials with controllable switches based on VO2," *Opt. Mater.*, vol. 114, 2021, Art. no. 110667.

[13] M. R. Akram, G. Ding, K. Chen, Y. Feng, and W. Zhu, "Ultrathin single layer metasurfaces with ultra-wideband operation for both transmission and reflection," *Adv. Mater.*, vol. 32, no. 12, 2020, Art. no. 1907308.

[14] M. R. Akram, M. Q. Mehmood, X. Bai, R. Jin, M. Premaratne, and W. Zhu, "High efficiency ultrathin transmissive metasurfaces," *Adv. Opt. Mater.*, vol. 7, no. 11, 2019, Art. no. 1801628.

[15] Y. Jiang, M. Zhang, W. Wang, and Z. Song, "Reflective and transmissive cross-polarization converter for terahertz wave in a switchable metamaterial," *Phys. Scr.*, vol. 97, no. 1, 2022, Art. no. 015501.

[16] Y. Z. Cheng et al., "Ultrabroadband reflective polarization convertor for terahertz waves," *Appl. Phys. Lett.*, vol. 105, no. 18, 2014, Art. no. 181111.

[17] J. Zhao, Y. Cheng, and Z. Cheng, "Design of a photo-excited switchable broadband reflective linear polarization conversion metasurface for terahertz waves," *IEEE Photon. J.*, vol. 10, no. 1, Feb. 2018, Art. no. 4600210.

[18] R. T. Ako, W. S. Lee, M. Bhaskaran, S. Sriram, and W. Withayachumnankul, "Broadband and wide-angle reflective linear polarization converter for terahertz waves," *APL Photon.*, vol. 4, no. 9, 2019, Art. no. 096104.

[19] B. Yin and Y. Ma, "Broadband terahertz polarization converter with anomalous reflection based on phase gradient metasurface," *Opt. Commun.*, vol. 493, 2021, Art. no. 126996.

[20] B. Yin, Z. Xu, and Y. Ma, "Terahertz off-axis focus polarization converter based on metasurface," *Prog. Electromagn. Res. Lett.*, vol. 100, pp. 91–97, 2021.

[21] J. Zhu, Y. Yang, and S. Li, "A photo-excited broadband to dual-band tunable terahertz prefect metamaterial polarization converter," *Opt. Commun.*, vol. 413, pp. 336–340, 2018.

[22] Y. Cheng, X. Zhu, J. Li, F. Chen, H. Luo, and L. Wu, "Terahertz broadband tunable reflective cross-polarization convertor based on complementary cross-shaped graphene metasurface," *Physica E. Low Dimens. Syst. Nanostructures*, vol. 134, 2021, Art. no. 114893.

[23] M. Zou, M. Su, and H. Yu, "Ultra-broadband and wide-angle terahertz polarization converter based on symmetrical anchor-shaped metamaterial," *Opt. Mater.*, vol. 107, Sep. 2020, Art. no. 110062.

[24] J. Huang, T. Fu, H. Li, Z. Shou, and X. Gao, "A reconfigurable terahertz polarization converter based on metal–graphene hybrid metasurface," *Chin. Opt. Lett.*, vol. 18, no. 1, 2020, Art. no. 013102.

[25] T. N. Cao, M. T. Nguyen, N. H. Nguyen, C. L. Truong, and T. Q. H. Nguyen, "Numerical design of a high efficiency and ultra-broadband terahertz cross-polarization converter," *Mater. Res. Exp.*, vol. 8, no. 6, 2021, Art. no. 065801.

[26] V. S. Yadav, S. K. Ghosh, S. Bhattacharyya, and S. Das, "Graphene-based metasurface for a tunable broadband terahertz cross-polarization converter over a wide angle of incidence," *Appl. Opt.*, vol. 57, no. 29, pp. 8720–8726, 2018.

[27] C. He and Z. Song, "Terahertz graphene metasurfaces for cross-polarized deflection, focusing, and orbital angular momentum," *Opt. Exp.*, vol. 30, no. 14, pp. 25498–25508, 2022.

[28] Z. Song, L. Zhang, and Q. H. Liu, "High-efficiency broadband cross polarization converter for near-infrared light based on anisotropic plasmonic meta-surfaces," *Plasmonics*, vol. 11, no. 1, pp. 61–64, 2016.

[29] N. K. Grady et al., "Terahertz metamaterials for linear polarization conversion and anomalous refraction," *Science*, vol. 340, no. 6138, pp. 1304–1307, 2013.

[30] J. Xu, R. Li, S. Wang, and T. Han, "Ultra-broadband linear polarization converter based on anisotropic metasurface," *Opt. Exp.*, vol. 26, no. 20, pp. 26 235–26 241, 2018.

[31] D. Chandu and S. Karthikeyan, "A miniaturized broadband high-impedance surface with flexible circular polarization sense," *IEEE Trans. Antennas Propag.*, vol. 67, no. 4, pp. 2819–2824, Apr. 2019.

[32] C. Gandhi, P. R. Babu, and K. Senthilnathan, "Designing a broadband terahertz half-wave plate using an anisotropic metasurface," *J. Infrared Millim. Terahertz Waves*, vol. 40, no. 5, pp. 500–515, 2019.

[33] T. Lu, P. Qiu, J. Lian, D. Zhang, and S. Zhuang, "Ultrathin and broadband highly efficient terahertz reflective polarization converter based on four l-shaped metamaterials," *Opt. Mater.*, vol. 95, Sep. 2019, Art. no. 109230.

[34] N.-H. Shen et al., "Optically implemented broadband blueshift switch in the terahertz regime," *Phys. Rev. Lett.*, vol. 106, no. 3, 2011, Art. no. 037403.

[35] Y. Cheng, R. Gong, and J. Zhao, "A photoexcited switchable perfect metamaterial absorber/reflector with polarization-independent and wide-angle for terahertz waves," *Opt. Mater.*, vol. 62, pp. 28–33, 2016.